Development of a porous burner for low calorific gaseous fuels offering a wide operating range

C. Wieland[*,1], P. Weinbrecht[1], C. Weis[1], P.Habisreuhter[1], D. Trimis[1]

[1]Engler-Bunte-Institute Combustion Technology (EBI-vbt), Karlsruhe Institute of Technology, Karlsruhe, Germany

Abstract

This work presents the development of a burner for the utilization of low calorific value waste gas, as it arises in the production of high purity hydrogen from biogas using an oxidative steam reforming process. Stable combustion of different fuel gases with fluctuating gas composition over a wide operating range is assured by the application of combustion in an inert porous medium (PIM) utilizing a kinematic flame stabilization mechanism. The development of the PIM-burner bases on calculated effective flame speeds within PIM derived from a 1-D numerical model including harsh operating conditions with preheating temperatures above 800 K and carbon dioxide concentration of 70 %-vol in the fuel gas. Experiments are conducted on a tailored test rig in order to validate numerical predictions by comparison of calculated effective flame speeds to effective flame speeds derived from temperature measurements in PIM.

Introduction

Low calorific gas, also known as lean gas, describes a category of gas mixtures showing heating values considerably lower than that of natural gas. Such low calorific gases occur e.g. in purification processes as a byproduct or as a so called biogas from digesters and landfills [1]. Utilization or treatment of such gases depends on the scale of the application and ranges from utilization as a resource in industrial gas production plants [2] over combustion in micro gas turbines [3] to flaring off [4].

The incineration and enthalpy valorization of low calorific waste gases in technical applications offers potential to make processes more efficient, save over-all energy consumption, reduce emissions related to heat provision and reduce production costs. One challenge in the implementation of such burners is the need for a certain operating range regarding fluctuations in flow rate and/or composition of feed streams and operation under secondary fuels, as waste streams are not available during e.g. start-up; additionally, power modulation is required e.g. for partial load operation.

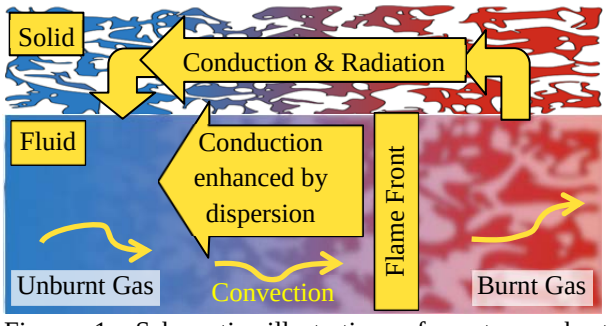

Figure 1: Schematic illustration of upstream heat transport in porous media, adapted from [5]

The burner developed within the present paper is related to a biogas-to-hydrogen processor, where low calorific gas is a byproduct of hydrogen purification. The so called offgas (OG) consists mainly of 70 %-vol CO_2, 21 %-vol H_2 and has a lower heating value of 2 MJ/kg. For start-up procedure the available plant feed biogas (BG) is used as an alternative fuel, which is modeled as mixture of 60 %-vol CH_4 and 40 %-vol CO_2, resulting in a lower heating value of 18 MJ/kg. Further details regarding fuel specifications can be found in Table 1.

Table 1: Composition, lower heating value (LHV) and burner inlet conditions for both fuels offgas and biogas

	Units	Offgas	Biogas
CO_2	%-vol	70.4	40
CH_4	%-vol	1.2	60
N_2	%-vol	0.8	
H_2O	%-vol	5.0	
H_2	%-vol	20.9	
CO	%-vol	1.7	
LHV	MJ/kg	2	18
T_{in}	K	823	453
ϕ	-	0.833	0.588

In the present work, the approach of porous burners is followed to perform combustion of low calorific gas. Due to thermal inertia of the solid matrix, possible fluctuations in offgas composition do not affect the flame stabilization. Thermal conductivity of the solid matrix, radiative heat transfer and the effect of dispersion contribute to an upstream heat transfer from the hot post flame front zone to the cold pre flame front zone as illustrated in Figure 1. This effect leads to an increased effective flame speed S_{eff} that is an important parameter for the design of the burner. S_{eff} depends on gas inlet temperature T_{in}, fuel composition and equivalence ratio ϕ; these process parameters also determine the combustion temperature.

The process of hydrogen purification sets the fuel composition, parameters T_{in} and ϕ have to be defined. With a view on plant components subsequent to the burner, a high flue gas temperature is preferred for efficient heat transfer. However, the introduction of a solid material into the flame zone involves limitations in the flame temperature. For silicon infliltrated silicon carbide (SiSiC) the maximum service temperature is 1723 K [6]; thus an adiabatic flame temperature of

* Corresponding author: christoph.wieland@kit.edu

1673 K is targeted in the determination of inlet conditions.

For offgas, an equivalence ratio $\phi_{OG} = 0.833$ is set to assure lean combustion regime and to have a mass flow that provides sufficient sensible heat for the subsequent heat exchanger system. With offgas composition, equivalence ratio and target temperature defined, the mixture inlet temperature is calculated to $T_{in,OG} = 823\ K$ in an enthalpy balance.

Biogas is used as an alternative fuel during start-up procedure. Mass flow of biogas is set to the value, providing the same power as that of offgas $\dot{m}_{BG} = \dot{m}_{OG} \cdot LHV_{OG} \div LHV_{BG}$. The equivalence ratio is set to $\phi_{BG} = 0.533$ in order to have a mass flow of air in the same scale as in offgas operation; thus the corresponding inlet temperature is $T_{in,BG} = 453\ K$.

Numerical Methods

Numerical methods focus on the calculation of one-dimensional flame profiles based on GRI3.0 detailed chemical reaction mechanism [7]. The applied model developed by Mendes et al. [8] represents an extended version of the widely used Chemkin PREMIX [9] code. Balance equations for the conservation of mass, species and enthalpy in the gaseous phase are solved (EQ 1-3). An additional balance (EQ 4) is introduced for the conservation of enthalpy in the solid phase.

$$\frac{d\dot{m}}{dx} = 0 \tag{1}$$

$$\dot{m}\frac{dY_k}{dx} + \frac{d}{dx}\left(\varphi A \rho_g D_k Y_k\right) - \varphi A\, RR_k M_k = 0 \tag{2}$$

$$\dot{m} c_{p,g}\frac{dT}{dx} - \frac{d}{dx}\left(\varphi A\, \lambda_{eff,g}\frac{dT_g}{dx}\right) + A\, H_v\left(T_g - T_s\right) + \varphi A \sum_k \rho_g c_{p,k} D_k \frac{dT_g}{dx} + \varphi A \sum_k RR_k\, h_k\, M_k = 0 \tag{3}$$

$$-\frac{d}{dx}\left(A\, \lambda_{eff,s}\right) - A\, H_v\left(T_g - T_s\right) + \frac{d(A\, Q_r)}{dx} = 0 \tag{4}$$

With $\dot{m}$ denoting mass flow rate, x the spatial dimension, Y_k the mass fraction of the k-th species, φ the porosity, A the cross-sectional area, ρ_g the gas density, D_k the diffusive velocity, RR_k the reaction rate, M_k the molar weight and h_k the formation enthalpy of the k-th species. $c_{p,g}$ denotes the heat capacity of the gaseous phase, Q_r the radiative heat flux, T_g and T_s the temperature of gaseous and solid phase, respectively.

Thermal coupling of solid and gaseous phase is realized by employing a volumetric heat transfer coefficient H_v that is calculated according to [10] from the volumetric Nusselt number Nu_v

$$H_v = Nu_v \cdot \frac{\lambda_g a_v}{l} \tag{5}$$

$$Nu_v = \mathrm{a} + \mathrm{b} \cdot Pr^c \cdot Re^d \tag{6}$$

using the specific surface area a_v, characteristic dimension l, dimensionless Prandtl and Reynolds numbers Pr and Re and PIM specific parameters a, b, c, d.

Effective thermal conductivity coefficients $\lambda_{eff,i}$ for gaseous and solid phase are calculated from pure solid's and mixture conductivity λ_s and λ_g, respectively. Effective solid conductivity takes into account the porous character of the solid body according to Kaviany [11]

$$\lambda_{eff,s} = (1 - \varphi)\lambda_s \tag{7}$$

Within the effective gas conductivity, axial dispersion of heat within the gaseous flow is modeled as descriped by Kaviany [11] and Voss [12], including the Peclet number Pe and a factor K_{ax}, which is depending on the porous structure:

$$\lambda_{eff,g} = \lambda_g\left(1 + \frac{Pe}{K_{ax}}\right) \tag{8}$$

Radiative heat transport is modeled within the solid phase using a discrete ordinate S-2 approximation [13], [14].

$$\frac{dQ_r}{dx} = (1 - \omega)\beta(4\sigma_{SB}T_s^4 - 2\pi\sum_{k=1} I_k) \tag{9}$$

With ω denoting the scattering albedo, β the extinction coefficient, σ_{SB} the Stefan-Boltzmann constant and I_k the radiation intensity of the k-th neighbor.

Setup of numerical studies started with an initial grid of 35 points and a mixture averaged diffusion model without consideration of thermal diffusion. Absolute and relative tolerances were set to 10^{-9} and 10^{-4} respectively. Adaptive grid parameters were gradually reduced from 0.9 to a value of 0.02 for gradient and curvature, resulting in final grids of 700 to 1000 points.

Numerical determination of laminar flame speed can be performed by calculating inlet flow velocity in a domain of constant cross-sectional area [15]. The numerical model used within this work takes into account a varying cross-sectional area arising from the conical divergent shape of the porous structure. Determination of effective flame speed was performed by finding the location of the flame front at the location of maximum OH concentration. The inlet velocity was translated from the inlet diameter to the diameter at flame front location.

$$S_{eff,num} = u_{in} \cdot \frac{A_{in}}{A(x(OH_{max}))} \tag{10}$$

Experimental Setup

Experiments are carried out using a tailored combustion test rig, designed to provide a multi-component fuel gas with a defined composition. Four thermal mass flow controllers from BRONKHORST HIGH-TECH B.V., Netherlands are used to accurately control the flow rates of four feed component streams of hydrogen, methane, carbon monoxide and carbon dioxide. The flow of the corresponding combustion air is controlled by a manual valve and monitored using a thermal mass flow sensor from Höntzsch GmbH, Germany. The streams of air and carbon dioxide can be electrically preheated up to 600 °C through two 17 kW electrical heaters 10000 DF from Leister, Germany. In order to measure the temperature profile along the flow direction of the PIM burner, ten S-Type thermo-couples with a protective tube of ceramic C799 from Rössel-Messtechnik GmbH, Germany are inserted into the porous structure that is produced by EngiCer SA, Switzerland. The porous structure is a conical shaped ceramic foam made of silicon infiltrated silicon carbide with pore density of 10 pores per inch (PPI). The PIM is positioned in an insulating counterpart made of a ceramic fiber vacuum molded body by Contherm Wärmedämmsysteme GmbH, Germany. A schematic illustration of the test rig setup is given in

Figure 2.

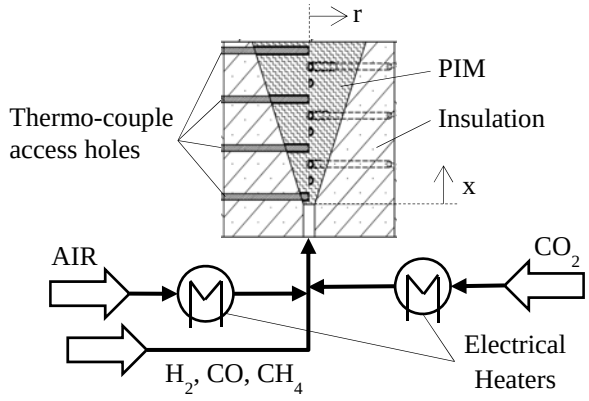

Figure 2: Schematic visualization of the test rig

Determination of effective flame speed from experimental data is performed by relating the inlet volumetric flow rate $\dot{V}_{in}$ to the cross-sectional area A of the burner at the axial position of the flame x_{flame}. Experimental data provide information regarding the temperature profile within the PIM; therefore, the criterion of maximum slope in the temperature profile $x_{flame} = x\left(\max\left\{\frac{\partial T}{\partial x}\right\}\right)$ is used to locate the flame front. Applying the ideal gas equation for retrieving $\dot{V}_{in}$ yields in

$$S_{eff,exp} = \dot{m}\frac{\mathbb{R}\,T_{in}}{p_{in}\,\bar{M}_{in}} \cdot \frac{1}{A\left(x\left(\max\left\{\frac{\partial T}{\partial x}\right\}\right)\right)} \tag{11}$$

With $\mathbb{R}$ denoting the ideal gas constant and $T_{in}, p_{in}, \bar{M}_{in}$ inlet temperature, pressure and mean molar weight, respectively.

Temperature information of experimental dataset is no continuous profile but discrete monitoring points, introducing uncertainty regarding the flame location δx_{flame}. With $x = 0$ at the inlet surface of the porous structure and linear relation of axial position x and PIM's radius r, EQ 11 can be transformed into

$$S_{eff} \propto A^{-1} \propto (0.365 \cdot x + 6\,mm)^{-2} \tag{12}$$

Derivation with respect to x and multiplication by uncertainty of flame location δx_{flame} yields in uncertainty of the effective flame speed $\delta S_{eff,exp}$

$$\delta S_{eff,exp} = \frac{\partial S_{eff,exp}}{\partial x} \cdot \delta x_{flame} \tag{13a}$$

$$\delta S_{eff,exp} \propto -\frac{\delta x_{flame}}{(0.365 \cdot x_{flame} + 6\,mm)^3} \tag{13b}$$

EQ 13b clearly demonstrates the dependency of the uncertainty in the effective flame speed from the actual location of the flame within the conical burner. Location of the flame near the inlet (low values for x_{flame}) introduce a high value in $\delta S_{eff,exp}$. The uncertainty in the effective flame speed arising from uncertainty of the flame position is dominating over other uncertainties; thus the error bars in Figure 6 and Figure 7 are based on the explained consideration.

Results

For the kinematic flame stabilization mechanism, the flow of premixed gas is led through a porous structure with increasing cross-sectional area, resulting in a decreasing gas velocity u_g along the porous structure. The flame is expected to stabilize at the location where $u_g = S_{eff}$. In order to determine the dimensions of the porous structure, the range of effective flame speeds and corresponding volumetric flow rates of premixed fuel and air must be known to determine a range of cross-section areas required depending on the operating conditions.

Development of the burner in the present work is based on 10 PPI random foam SiSiC as this structure is widely used in porous burner applications and characteristic values are available in literature [16], [13]. A summary of used values is given in Table 2.

Table 2: List of simulation parameters for 10 PPI SiSiC random foam

a	0.3
b	0.664
c	0.333
d	0.5
K_{ax}	0.55
l	0.06 cm

ϵ	0.90
a_v	5 cm-1
ω	0.7
β	1 cm-1

In a first step, flame profiles of offgas and biogas under the conditions mentioned above in Table 1 were calculated by applying the numerical model and using 10 PPI SiSiC random foam parameters from Table 2. Using EQ (10) yields in effective flame speeds of $S_{eff,OG} = 14.22\,\frac{\mathrm{m}}{\mathrm{s}}$ and $S_{eff,BG} = 1.63\,\frac{\mathrm{m}}{\mathrm{s}}$.

The range of cross-sectional areas of the burner is determined through division of the volumetric flow rate

by the effective flame speed, with the volumetric flow derived from mass flow rate and actual inlet conditions

$$A = \dot{m}\,\frac{\mathbb{R}\,T_{in}}{p_{in}\,\bar{M}_{in}} \cdot \frac{1}{S_{eff}} \qquad (14)$$

Mass flow rate, inlet temperature, corresponding volumetric flow rate, effective flame speed and resulting cross-sectional area and appropriate diameter are listed in Table 3 for offgas and biogas. Application of the burner in an industrial plant demands flexibility in power modulation, e.g. for partial load operation; thus, nominal flow rates ("high") are complemented by reduced flow rates ("low") for a turn-down ratio of 1:10 in Table 3.

Limits for the range of required diameter are set by offgas at turn-down with 19 mm and by biogas at nominal flow rate with 125 mm. The axial dimension of the PIM is set to 148 mm, resulting in a spacing of 15 mm between the temperature monitoring points.

Table 3: Summary of mass flow rate, inlet temperature, corresponding volumetric flow rates, effective flame speed and resulting stabilization diameter for different operating conditions

	$\dot{m}$	T	$\dot{V}$	S_{eff}	D_{req}
	kg/h	K	m^3/h	m/s	cm
Offgas (High)	105.2	823	153.5	14.2	6.2
Offgas (Low)	10.5	823	15.3	14.2	**1.9**
Biogas (High)	82.4	453	72.1	1.63	**12.5**
Biogas (Low)	20.2	298	11.7	1.63	5.0

Transferring the dimensions from Table 3 into a burner design results in the conical geometry shown in Figure 3, with the offgas flame at nominal flow rate located at an axial position in middle of the burner, offgas flame at turn-down flow rate located near the inlet and biogas flame at nominal flow rate located near the outlet of the porous structure.

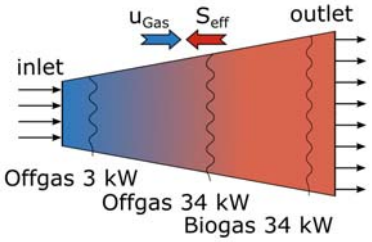

Figure 3: Schematic illustration of conical shaped porous burner with flame position under different operating conditions

Validation was performed by comparison of numerically gained results with experimentally obtained ones. Figure 4 shows the measured temperatures from experiment (square symbols) under biogas operation at an inlet temperature of 456 K and an equivalence ratio of 0.58 and the corresponding temperature profiles for solid and gaseous phase (solid and dashed line) from numerical calculation. Experimentally measured temperature profile matches with the numerical prediction for the solid phase. This congruency is reasonable due to radiative heat transfer between thermo-couple and PIM. Simulations show a pronounced peak in the gas temperature profile.

An offgas experiment with an inlet temperature of 637 K and equivalence ratio of 0.833 is presented in Figure 5 (squares) together with the corresponding numerically derived profiles for solid and gaseous phase (solid and dashed line). The flame front is indicated by a sharp rise in temperature. In contrast to the biogas experiment, measured temperatures in the hot zone downstream the flame front are significantly lower than the simulated values. Furthermore, no pronounced peak in the gas temperature is predicted for offgas operation.

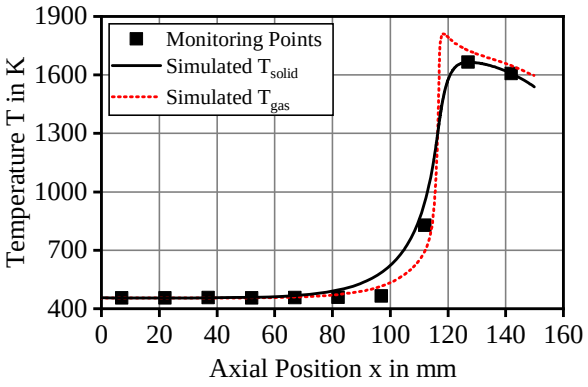

Figure 4: Axial temperature profile of biogas ($\phi = 0.588$; $T_{in} = 453\ K$), measured temperatures (black squares) and simulated profiles of solid phase (solid line) and gas phase (dashed line)

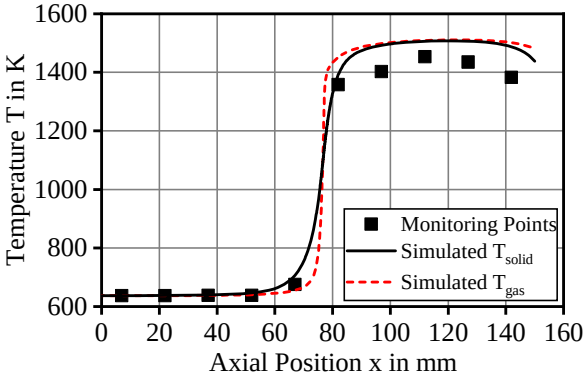

Figure 5: Axial temperature profile of offgas ($\phi = 0.833$; $T_{in} = 637\ K$), measured temperatures (black squares) and simulated profiles of solid phase (solid line) and gas phase (dashed line)

The effective flame speed is given as function of adiabatic flame temperature in Figure 6 and Figure 7. Results for combustion of biogas are summarized in Figure 6 with an equivalence ratio of $\phi_{BG} = 0.59$ at preheating temperatures ranging from 293 K to 456 K. Simulation results are ranging from 0.66 m/s to 1.63 m/s

for the effective flame speed. Experimental results for S_{eff} are ranging from 1.14 m/s to 1.88 m/s, consequently showing a positive offset to the numerical predicted values. Linear regression of the results in the range under consideration yields in a mean offset of 0.57 m/s for experimentally gained values from numerical predictions, corresponding to a mean relative deviation of 54 %.

Results for combustion of offgas are summarized in Figure 7 with an equivalence ratio of $\phi_{OG} = 0.83$ at preheating temperatures ranging from 594 K to 808 K. Results for the effective flame speed are ranging from 6.46 m/s to 14.2 m/s for numerical simulations and from 3.66 m/s to 18.8 m/s for experiments. For offgas no general offset from numerical to experimental results is found, linear regression lines are crossing within the considered range and show the same trend. Mean difference between numerically and experimentally determined effective flame speed of offgas is 1.3 m/s, corresponding to a mean relative deviation of 13 % that is considered as good agreement of measured values and numerical calculations. For the offgas experiments, significant variation of error bar size can be observed in Figure 7 with larger error bars at elevated effective flame speed. This is caused by the fact that an increased flame speed leads to a stabilization in the upstream part of the conical shaped burner where the cross-sectional area is smaller. For a smaller diameter, a constant uncertainty in the axial position implies an increased uncertainty in the corresponding velocity as shown in EQ (13b).

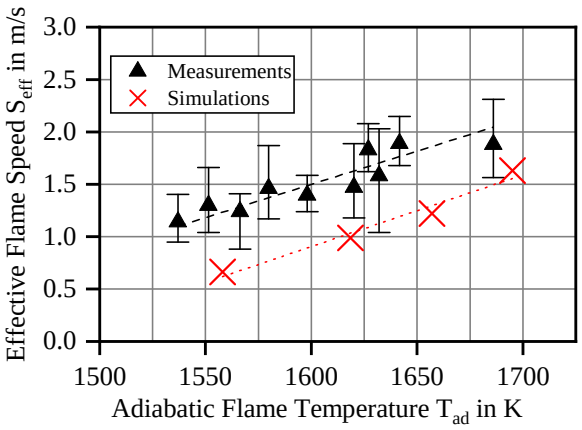

Figure 6: Effective flame speed of biogas within 10 PPI SiSiC random foam as function of fuel-air mixture's adiabatic flame temperature; simulations with $\phi = 0.588$.

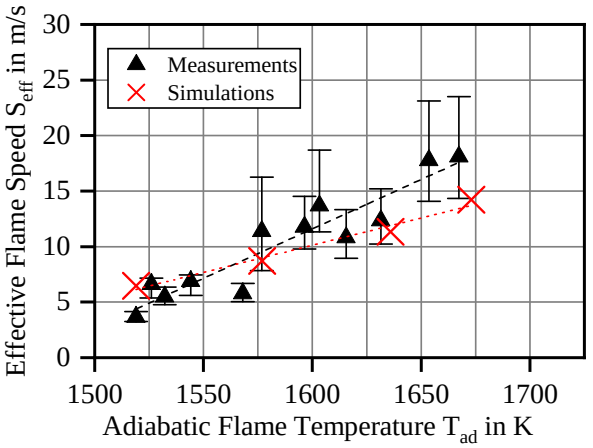

Figure 7: Effective flame speed of offgas in 10 PPI SiSiC random foam as function of adiabatic flame temperature; simulations with $\phi = 0.833$.

A potential cause for the deviation in the results lies in the composition of the considered mixtures. Offgas is a H_2 based fuel and biogas is based on CH_4; thus, the combustion process is diffusion-determined in the first case and controlled by heat conductivity in the latter one. However, PIM's influence on the flow field is modeled simply by an increased conductivity of the gaseous phase as shown in EQ 8. Furthermore, the PIM parameters of Table 2 are retrieved from literature and not from the actual sample of SiSiC that was used in the experiments.

Conclusions

The combustion of low calorific value gases with varying composition and heating value is an important measure for the improvement of chemical processes' efficiency. A promising approach to the combustion of such gases is the application of porous burners. In the present work, a 1-D numerical model was applied in order to develop a porous burner, capable of processing two different fuels in a wide modulation range. The present study deals with one fuel composed mainly of CO_2 and H_2 with a lower heating value of 2 MJ/kg, and another one composed of CH_4 and CO_2 with a heating value of 18 MJ/kg. Results of the design process were transferred into a prototype burner that was tested in order to validate the numerical predictions. For biogas, temperature profiles of numerical simulation and experiment show good agreement, yet an offset is observed for the derived effective flame speed. In contrast to this, offgas temperature profiles show deviations from simulated to measured values while results for the effective flame speed show good agreement. Despite the observed deviations between simulations and experiments, extrapolation of the existing model to the conditions in the present case and dimensioning of a burner for a technical application was successful.

Acknowledgements

The results presented in this article have been elaborated within the EU project BioRobur^{plus}. This

project has received funding form the Fuel Cells and Hydrogen 2 Joint Undertaking under grant agreement No 736272. This Joint Undertaking receives support from the European Union's Horizon 2020 research and innovation program and Hydrogen Europe and N.ERGHY.

References

[1] E.-J. Nyns, M. Nikolausz and J. Liebertau, "Biogas," in *Ullmann's Encyclopedia of Industrial Chemistry*, Weinheim, Wiley-VCH Verlag GmbH & Co. KGaA, 2014, pp. 1 - 14.

[2] W. Boll, G. Hochgesand, C. Higman, E. Supp, P. Kalteier, W.-D. Müller, M. Kriebel, H. Schlichting and H. Tanz, "Gas Production, 3. Gas Treating," in *Ullmann,s Encyclopedia of Industrial Chemistry*, Weinheim, Wiley-VCH Verlag GmbH & Co. KGaA, 2012, pp. 483 - 539.

[3] J. Leicher, A. Giese, K. Görner, V. Scherer and T. Schulzke, "Development of a Burner System for Use of Low Calorific Fuel Gases in Micro Gas Turbines," in *Proceedings of the European Combustion Meeting*, 2011.

[4] A. Bahadori, Pollution Control in Oil, Gas and Chemical Plants, Cham Heidelberg New York Dordrecht London: Springer, 2014.

[5] C. Bedoya, I. Dinkov, P. Habisreuther, N. Zarzalis, H. Bockhorn and P. Pathasarathy, "Experimental study, 1D volume-averaged calculations and 3D direct pore level simulations of the flame stabilization in porous inert media at elevated pressure," *Combustion and Flame*, no. 162, pp. 3740 - 3754, 2015.

[6] S. Gianella, D. Gaia and A. Ortona, "High temperature applications of Si-SiC cellular ceramics," *Advanced Engineering Materials*, December 2012.

[7] G. P. Smith, D. M. Golden, M. Frenklach, N. W. Moriarty, B. Eiteneer, M. Goldenberg, C. T. Bowman, R. K. Hanson, S. Song, W. C. Gardiner, V. V. Lissianski and Z. Qin, "GRI-Mech 3.0," [Online]. Available: http://www.me.berkeley.edu/gri_mech/.

[8] M. Mendes, J. Pereira and J. Pereira, "A numerical study of the stablility of one-dimensional laminar premixed flames in inert porous media," *Combustion and Flame*, no. 153, pp. 525 - 539, 2008.

[9] R. Kee, F. Ruplex, J. Miller, M. Coltrin, J. Grcar, E. Meeks, H. Moffat, A. Lutz, G. Dixon-Lewis, M. Smooke, J. Warnatz, G. Evans, R. Larson, R. Mitchell, L. Petzold, W. Reynolds, M. Caracotsios and W. Stewart, *CHEMKIN Collection*, Release 3.6 ed., I. Reaction Design, Ed., San Diego, CA, 2000.

[10] S. Voss, M. Mendes, J. Pereira, S. Ray, J. Pereira and D. Trimis, "Investigation on the thermal flame thickness for lean premixed combustion of low calorific H2/CO mixtures within porous inert media," *Proceedings of th Combustion Institute*, no. 34, pp. 3335 - 3342, 2013.

[11] M. Kaviany, Principles of heat transfer in porous media, vol. 2nd ed., New York: Springer, 1999.

[12] S. Voß, Verbrennung von Wasserstoff und Synthesegasgemischern, Aachen: Shaker Verlag, 2014.

[13] Mendes, *Modeling and Simulation of Hydrocarbon Oxidation Processes within Porous Inert Media*, Instituto Superior Técnico, Technical University of Lisbon, 2011.

[14] M. Modest, Radiative Heat Transfer, vol. 2nd ed., Amsterdam, Boston: Academic Oress, 2003.

[15] Reaction Design, *PREMIX*, vol. Chemkin Collection Release 3.6, 2000.

[16] M. Scheffler and P. Colombo, Cellular Ceramics, Weinheim: WILEY-VCH Verlag GmbH & Co. KGaA, 2005.